Proceedings of the ASME 2014 Power Conference
POWER2014
July 28-31, 2014, Baltimore, Maryland, USA

POWER2014-32052

NUMERICAL INVESTIGATION OF ROTATING STALL CHARACTERISTICS AND ACTIVE STALL CONTROL IN CENTRIFUGAL COMPRESSORS

Taher Halawa
Mechanical Engineering Department, UBC-University of British Columbia, Vancouver, B.C., Canada

Mohamed Alqaradawi
Mechanical & Industrial Engineering Department, Qatar University, Doha, Qatar

Osama Badr
Mechanical Engineering Department, British University, Cairo, Egypt

Mohamed S. Gadala
Mechanical Engineering Department, UBC-University of British Columbia, Vancouver, B.C., Canada

ABSTRACT

This paper focuses on providing better view for the understanding of rotating stall phenomenon in centrifugal compressors by using numerical simulations and presents a study of the role of air injection method in delaying stall inception by using different injection parameters aiming at increasing the efficiency of this method. Results showed that the formation of stall begins at the impeller inlet due to early flow separation at low mass flow rates and due to the increase of the turbulence level and the absence of fluid orientation guidance at the vaneless region. The flow weakness causes back flow that results in the formation of the tip leakage flow which causes stall development with time. Results also showed that using air injection at specified locations at the vaneless shroud surface at injection angle of 20° and with injection mass flow rate of 1.5% of the inlet design mass flow rate, can delay the stall onset to happen at lower mass flow rate about 3.8 kg/s comparing with using injection with angle of 10° with different injection mass flow rates and also comparing with the case of no injection.

1. INTRODUCTION

The compressor stability depends on the compressor operating condition. If the compressor works at a condition between the choke limit and the surge limit, then the compressor is in the stable zone. Also, there is an unstable zone which is called the rotating stall and surge region and is located at low mass flow rate close to the surge line. At the stall region, the compressor is completely unstable, and there is high pressure fluctuations affecting the blades. The early flow separations cause formation of vortices and low velocity regions or stall regions which can increase with time resulting in the development of stall into surge or back flow.

Stall inception types are classified into two categories; the modal stall inception and the spike stall inception. Modal stall disturbances or modes are characterized by the formation of small amplitude disturbances that grow with long length scale in the axial direction. These modes can appear at hundreds of impeller revolutions before stall initiation [1-3]. The modal stall inception occurs at a condition when the slope of the stagnation to static pressure curve for the compressor performance map is zero [4]. The spike stall inception, studied in the present paper, is defined as the formation of finite amplitude disturbances at blade tips, and these disturbances can increase its size very quickly within approximately five impeller revolutions. The spike stall inception was found to appear when the slope of the stagnation to static pressure curve with the mass flow rate is negative [5].

The identification of rotating stall features provides a good view about the reasons of stall onset and its development, and it was found that the early separation, tip leakage flow and pressure fluctuations at blade tips and at the vaneless region are the main signs of rotating stall and can be developed into surge [6-8]. The tip leakage flow can interact with the inlet flow and then the interface between these flows can be perpendicular to the inlet flow direction when the stall is developed [9]. Vo et al. [10] clarified that There is a connection between the formation of the tip leakage flow and the development of stall due to the initiation of back flow from diffuser at some impeller passages resulting from the turbulence of the tip leakage vortex.

When the compressor works near stall condition, there is a periodic variation of pressure at blade surfaces, and this leads to the collapse of vortices at blade tips resulting in the motion of the tip leakage flow to block the flow at inlet [8]. Geng et al. [11] performed a numerical simulation of rotating stall development in a low speed isolated axial flow compressor by using numerical model with variable exit boundary condition which is used to simulate the effect of valve closure. It was noted that spike stall is initiated with the formation of two vortices at impeller inlet; one of them is moving from one impeller passage in a reversed direction to another passage, while the other vortex is extended in the radial direction and impacting the blade suction side. Vagani et al. [12] studied the prediction of rotating stall onset for a high speed centrifugal compressor using numerical simulations. Results showed that the main reason of stall is the increase of flow incidence angle at impeller inlet, while the stall is developing due to the formation of reversed flow at some locations near the impeller leading edge.

One of the most successful methods to increase the compressor stable margin is the air injection method. In the air injection method, external air is injected at high speed using nozzles which are fixed at some locations near the blades tip in order to interact with the stall regions and correct the fluid velocity magnitude and direction. For axial compressors, the injection location is mostly close to the impeller blade tip leading edge at the shroud surface.

Beheshti et al. [13] used a numerical model that combines casing treatment with air injection for a high speed transonic axial compressor in order to increase the compressor stable range. It was found that using this model at injection mass flow rate of 2.4% of the design inlet mass flow results in improving the surge margin by 7% and increasing the maximum efficiency by 0.8% comparing with the case without treatment and without air injection. Khaleghi et al. [14] made a numerical investigation about the effect of changing the velocity of injection at blades tip on the stability range of an axial high speed compressor. Results indicated that using of injection velocity equals to sonic speed value achieves minimum pressure fluctuations and minimum blades loading. Benhegouga and Ce [15] made an optimization of the air injection parameters as injection mass flow rate, injection position and injection angle for a transonic axial compressor. Numerical results showed that the stall margin is increased by increasing the injection mass flow rate and by using injection Yaw angle between -20° and -30°.

For centrifugal compressors, the air injection at the vaneless region between the impeller and diffuser is recently used to increase the surge margin. There are series of successful experiments done about the air injection on the NASA CC3 centrifugal compressor which is selected to be simulated in the current study, because there are several numerical and experimental studies done on this compressor [7, 16-21].

Skoch [17] measured the performance of the NASA CC3 compressor when using external air injection at the hub surface of the vaneless region. The air was injected in three directions; towards the suction side of the diffuser vanes, towards both suction and pressure vane sides and in the direction of vane pressure side. Measurements showed that there is a very small improvement in the surge margin when injecting air towards the vanes pressure side; and results also referred to that the air injection at the shroud surface can be more beneficial than the injection at the hub surface. Skoch [18] made an accurate measurements on the NASA CC3 centrifugal compressor concerning the stabilization using air injection at the vaneless region. External air was injected through 8 nozzles fixed at the shroud surface of the vaneless space, and the air was injected tangentially in the forward direction and in the reverse direction of impeller rotation. The experimental results showed that the forward tangent injection is better than the reverse tangent injection in terms of improving the surge margin and decreasing the pressure losses. By using the forward tangent injection at mass flow rate of 0.9% of the design inlet mass flow rate, the surge margin is increased to 13.4% and the pressure losses were decreased to 1% relative to the maximum pressure of the compressor design curve.

The main aim of the current study is to simulate the rotating stall phenomenon in order to provide a better view of the stall features and the development process of stall with time. Also, this study is focusing on the air injection method and its role in increasing the compressor stability zone and decreasing the unstable forces acting on the blades during stall.

2. DESCRIPTION OF THE CASE STUDY

The selected compressor for this study is the NASA CC3 transonic centrifugal compressor. Figure 1 shows this compressor with its internal main components.

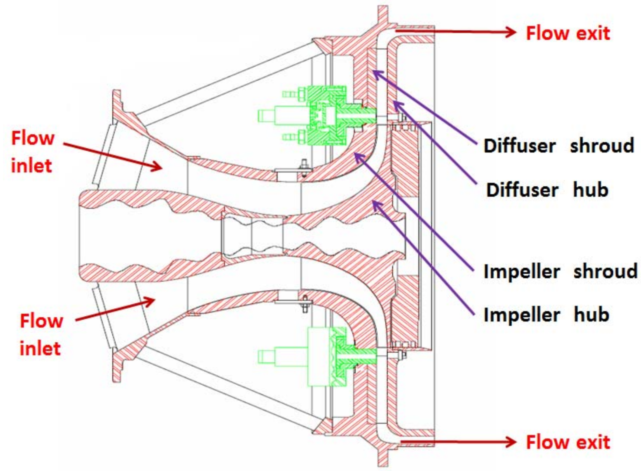

Figure 1. NASA CC3 compressor configuration [18]

The impeller is composed of 15 main blades and 15 splitter blades with back sweep of 50 degrees from radial at impeller exit. The impeller inlet and exit tip diameters are 210 mm and 431 mm respectively. The diffuser shape is vane island and is composed of 24 vanes. The diffuser vane leading edge is located at diameter ratio of 1.08, while the vane trailing edge is at diameter ratio of 1.68 corresponding to the impeller exit diameter. The design conditions of this compressor are rotational speed of 21,789 revolutions per minute, pressure ratio of 4 and mass flow rate of 4.54 kg/s. McKain and Holbrook [22] provided geometrical details and design parameters for the NASA CC3 compressor including performance maps and blade loading curves and structural analyses.

3. NUMERICAL METHODOLOGY

In this study, FLUENT [23] was utilized to solve the continuity, energy, Navier Stokes and turbulence equations. The solution method used is the sliding mesh in which the flow zones are divided into rotating zones, static zones and deforming zones and there are interface surfaces between the rotating and static zones. The mesh is modified at the end of each time step during solution. Equation 1 describes the way that the mesh volume is to be calculated.

$$V^{n+1} = V^n + \frac{dV}{dt}\Delta t \qquad (1)$$

Where V is the mesh volume, and n, $n+1$ are referring to the current and next time step values, respectively, and dV/dt is the volume time derivative of the control volume which can be calculated from the following equation:

$$\frac{dV}{dt} = \int_{\partial V} \vec{u}_g \cdot d\vec{A} = \sum_{j}^{n_f} \vec{u}_{g,j} \cdot \vec{A}_j \qquad (2)$$

where n_f is the number of faces on the control volume and A_j is the j^{th} face area vector and $\overline{u}_g$ is the mesh velocity of the moving mesh. The right hand side of equation 2 can be calculated from the following equation:

$$\vec{u}_{g,j} \cdot \vec{A}_j = \frac{\delta V_j}{\Delta t} \qquad (3)$$

Where δV_j is the volume swept out by the control volume j over the time step Δt. The turbulence model used is the realizable *k-ε* model, and the reason behind the selection of this model is that it can guarantee accurate simulations for high turbulent flow associated with strong separations because the equation of turbulent viscosity is related to the variation of velocity gradients due to sudden flow separations and vortices formation.

There are two numerical models used in this study; the first one is the single passage model and the second is the full annulus model. The single passage model (Fig.2) is composed of three main components of the compressor which are the inlet guide, impeller and diffuser, but each component is represented by part of the whole geometry or a single blade passage. The single passage model was used for the verification of the numerical results with measurements, and this type of verification does not need the solution of all blade passages, so that the using of this model saved the overall computational time.

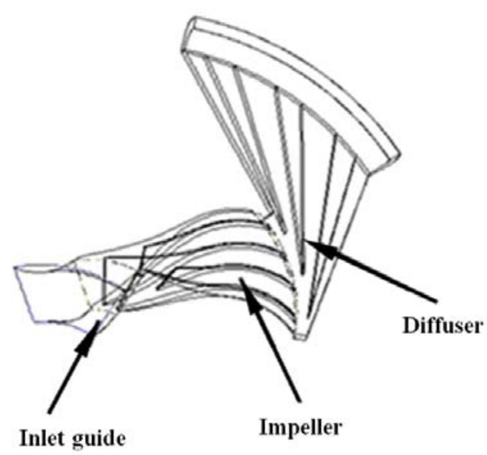

Figure 2. Single passage model

The full annulus model (Fig.3) is composed of all compressor parts with all blade passages included, and this model was used for the unsteady simulations of rotating stall because the distribution of the flow parameters varies from one blade passage to another, and the single passage model is not suitable for this kind of simulation.

The boundary conditions used in both models are pressures at inlet and exit boundary surfaces, and the numerical model was iterating to find the corresponding mass flow rate and this method was found to be accurate specially at high pressure ratios and low mass flow rates. There are interface surfaces between the rotating zones and the fixed zones; and the mesh is modified at the interface surfaces at each time step. In the case of the single passage model, there are periodic surfaces which are identical in shape and have the same flow parameters values because it is supposed that the periodic zones are repeated to complete the full geometry.

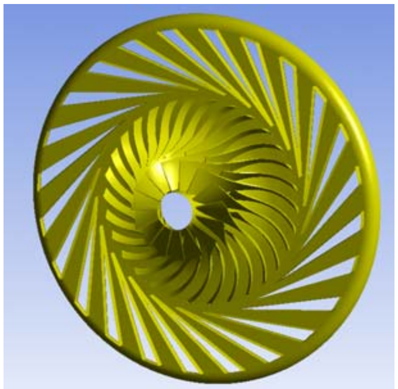

Figure 3. Full annulus model

4. MESH SENSITIVITY ANALYSIS

In order to verify the mesh accuracy, the following analysis was done to find the proper meshing parameters that will satisfy solution convergence and accurate results. In the purpose of studying the mesh sensitivity, several mesh sets were generated by varying parameters as the mesh growth rate, minimum mesh size and the number of mesh elements in the narrow gaps. The total number of mesh elements was increased by decreasing the mesh growth rate gradually from 1.5 to 1.1 and increasing the number of mesh elements in the narrow gaps from 3 to 8 mesh cells per gap, and also by decreasing the smallest mesh size on each face. In the process of increasing the number of mesh elements, the maximum cell skewness was monitored to ensure that the mesh quality is increasing and the average value of the maximum cell skewness was decreased from 0.3 to 0.14which is considered to be relatively a good value , because values close to 1 are causing problems in the solution stability. As the number of mesh elements increases, the variations of flow parameters decrease to the limit that they will be nearly constant corresponding to some values of mesh parameters. Figures 4 and 5 show the variation of density and Mach number, respectively with the number of mesh elements for the single passage model. It may be noted from figures 4 and 5 that by increasing the number of mesh elements more than 1.4 million has no further effect on the flow parameter values, and for that reason, the mesh set of 1.4 million cells was selected for making the simulations for the single passage model. On the other hand, similar mesh sensitivity analysis was done using the same procedure and it was found that about 15 million cells level is suitable for the full annulus model.

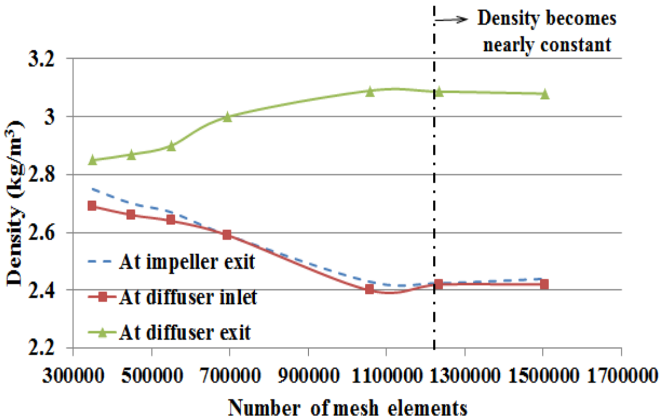

Figure 4. Density dependency on the mesh variation

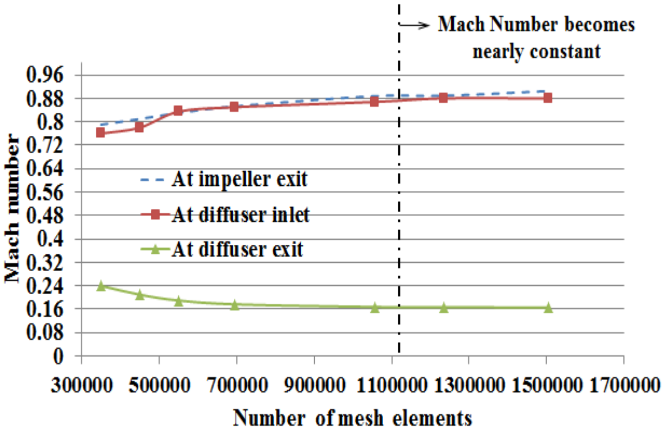

Figure 5. Mach number dependency on the mesh variation

5. RESULTS

5.1. Validation of the Numerical Model

The compressor pressure map is composed of total pressure ratio on the vertical axis and mass flow rate on the horizontal axis, and there are several speed lines including the design compressor speed. Figure 6 shows the compressor map of the NASA CC3 compressor according to previous measurements [19]. This map was selected to verify the numerical model results since it represents the final outcome of the numerical analysis. The single passage model was used to solve for some points for each speed curve in order to generate the complete map, and this was done for the design speed curve and for the 70%, 80% and 90% speed line curves. Figure 7 shows the compressor map according to the numerical model results.

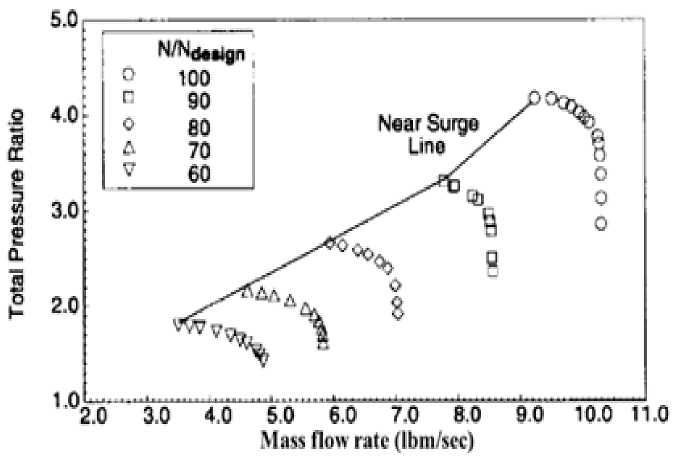

Figure 6. Pressure map (from measurements [19])

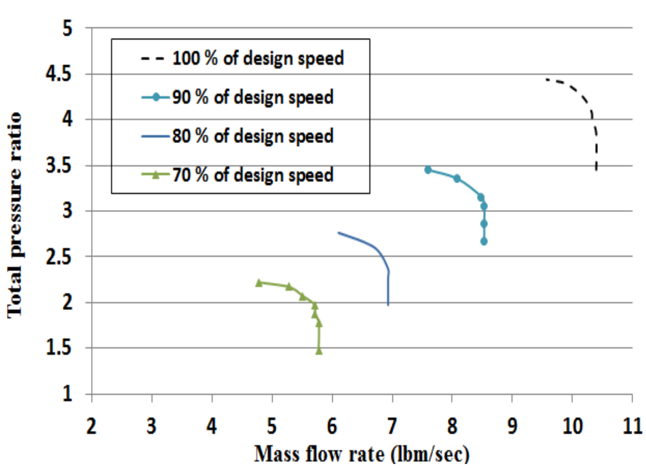

Figure 7. Pressure map (from numerical simulations)

For each operating condition on any speed line, the number of iterations per time step was 15 and the time step used is 4x10^{-6} sec using Courant number of 4 and with total number of iterations around 40,000. It can be seen from figures 6 and 7 that there is a good matching between computational results and measurements and there are regions with relative error around 4 % and this is only for points near the surge line and at high pressure ratios.

5.2. Simulation of Rotating Stall Using the Full Annulus Model

The rotating stall simulation was done at an operating condition in the unsteady region where the stall appearance is expected. Figure 8 shows the compressor map with indicating the location of the selected point for the stall simulations; this point is located at the left of the last stable point for the 21,789 rpm speed curve corresponding to mass flow rate of 3.8 kg/s, and this point is inside the unstable zone because its position exceeds the surge limit for the safe zone.

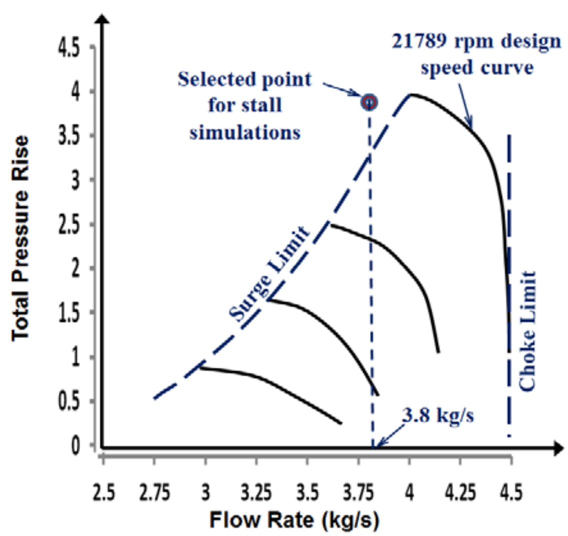

Figure 8. Location of point where stall is simulated

During the solution of this condition near the surge, the pressure values at the vaneless region between the impeller and diffuser were monitored with time to watch the pressure fluctuations. Figure 9 indicates the pressure values with time (in rotor revolutions) at 12 locations at the vaneless space, and it can be noted that the pressure is fluctuating with small amplitude for some time, and then the amplitude grows gradually with time until reaching a moment at which pressure starts to fluctuate strongly, and this indicates that the rotating stall occurs at this time and is developing.

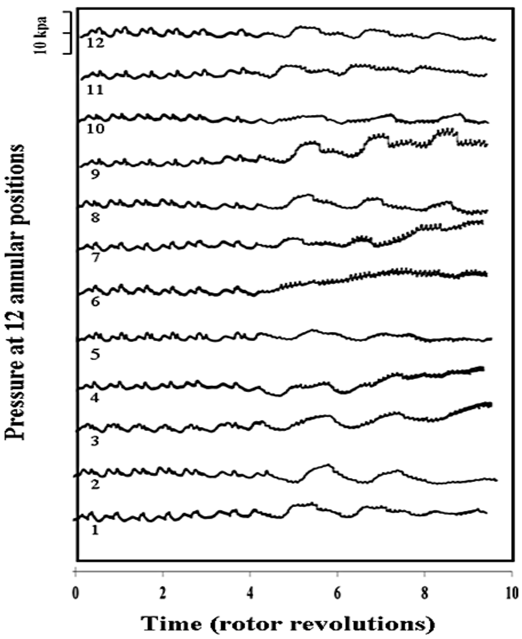

Figure 9. Pressure monitoring with time at the vaneless region

During the stall process, the velocity and pressure distributions are varying with time especially near the shroud surface where the stall cells initiated. Figure 10 indicates the pressure distribution at a plane of 95% of the span length at different time frames starting from the reference time at which stall is initiated and after 3, 5, 7 and 9 rotor revolutions from the reference time. It can be noted that pressure distribution is normal at the reference time with pressure ratio of 4:1, but after 3 revolutions, pressure distribution changes at the vaneless region between impeller and diffuser and this can be related to the velocity disturbances. After 5 revolutions, some localized high pressure regions appear at the vaneless region and that is because the fluid is impacting impeller blades; and these high pressure regions increase in size and number as can be seen after 7 and 9 revolutions.

The development of stall into the early stage of surge can be described in the form of main characteristics of the stall phenomenon. Due to weakness of the inlet axial flow velocity, separation occurs early causing turbulence and vortices in the impeller passages as shown in Fig.11 in which the velocity vectors are presented at a plane close to the shroud impeller surface during stall process, and it can be seen from the zoomed in area in figure 11 that the flow separation appears at the impeller leading edge followed by a stalled region.

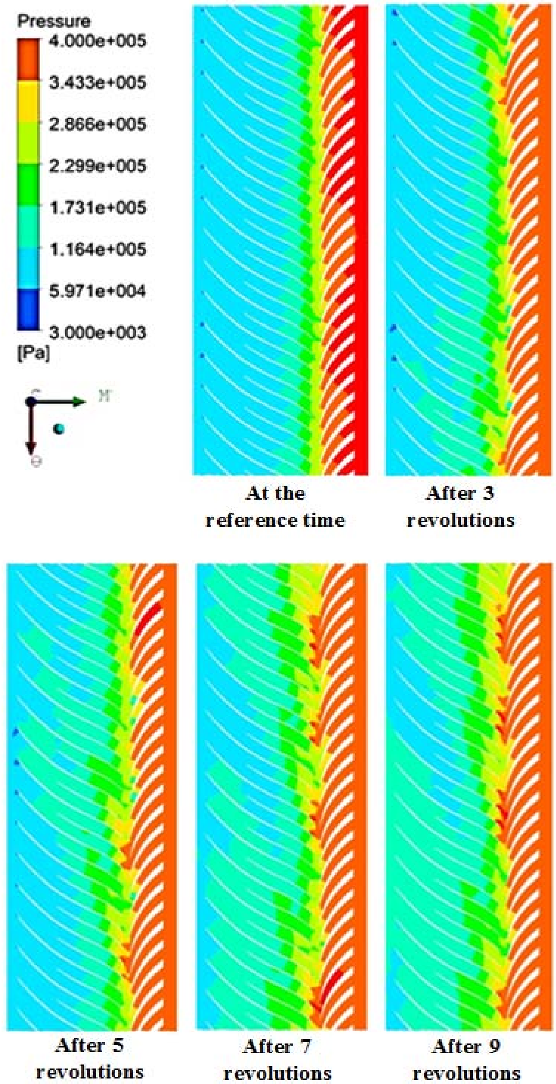

Figure 10. Pressure development during stall

The first main characteristic of the stall phenomenon is the occurrence of the tip leakage flow at which the fluid moves from blade pressure side to blade suction side across the clearance between the blades tip and shroud causing disturbance of the flow in the affected passage (Fig.12).

The second main characteristic of the stall phenomenon is the back flow impingement when the fluid at the rotor exit is turning back from one passage to another through the vanless region instead of transferring into the diffuser and this is causing fluid velocity deviation at the impeller exit as shown in Fig.13.

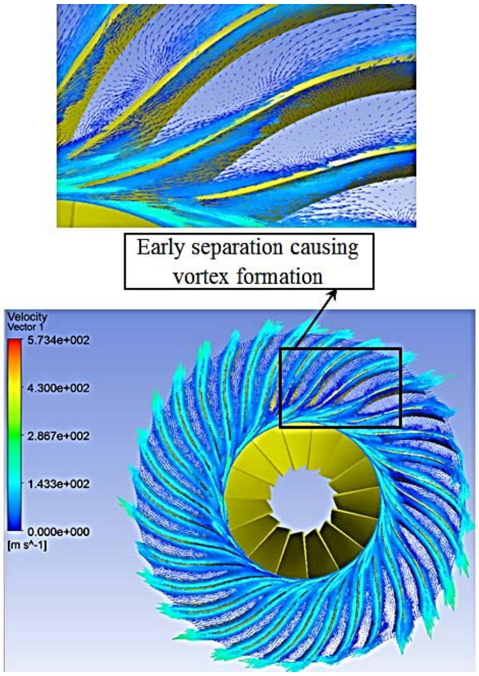

Figure 11. Velocity vectors near impeller shroud during stall

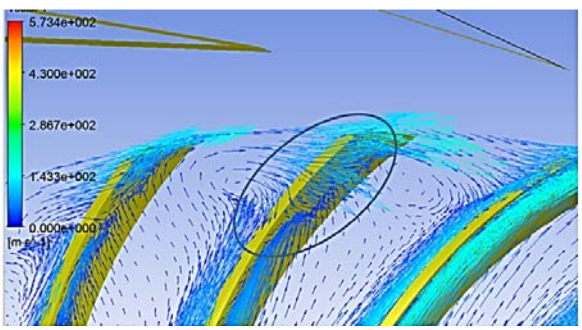

Figure 12. Velocity vectors showing tip leakage flow

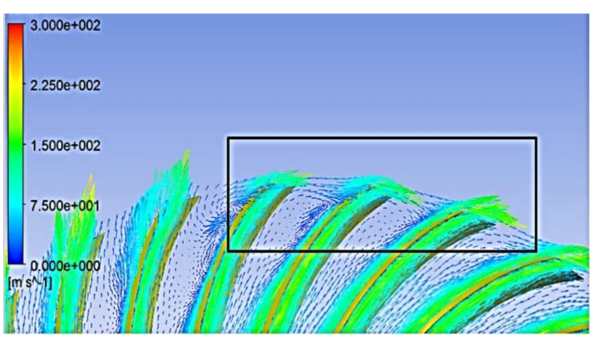

Figure 13. Velocity vectors showing back flow impingement at impeller exit during stall

The velocity deviation at the impeller exit causes the diffuser blockage or the failure of the fluid to enter the diffuser at the designed vane angle; and this causes the formation of very low velocity regions at diffuser entrance and it can be developed with time to form a back flow and this is considered the sign of beginning of surge. Fig.14 shows the velocity contours near diffuser shroud surface during stall, and it is clear that there are some diffuser passages with very low velocity values; and it is shown also in figure 14, the velocity vectors at part of the compressor (the area inside the rectangle shown), and the velocity vectors show the formation of back flow which is the reason for the low velocity values at this area.

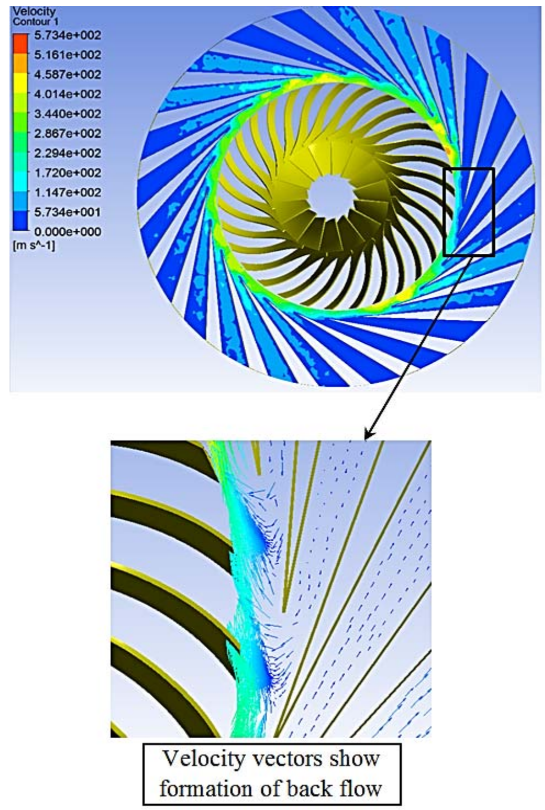

Figure 14. Velocity contours near diffuser shroud surface during stall

5.3. Air Injection Method Simulations

The idea of air injection is to inject relatively high speed flow at the vaneless region where the possibility of stall cells formation is high in order to treat these low velocity regions and prevent the back flow from diffuser into the impeller. The external air is injected at the vaneless region of the shroud surface at 12 equally spaced points as shown in Fig.15, and the reason behind this selection is that it was found that at least 8 injectors are required to ensure the successful air injection effect according to previous studies [17,18].

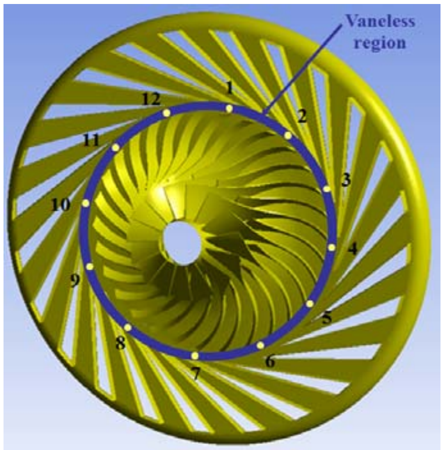

Figure 15. Description of the air injection locations

Two injection angles of 10° and 20° were selected to be studied and the injection angle is measured from the tangential direction as indicated in Fig.16. This selection is aiming to compare the effect of injecting air towards the suction side and pressure side of the diffuser vanes because the inlet diffuser vane angle is 15°. The air was injected at three mass flow rate values; 0.7%, 1% and 1.5 % of the compressor design inlet mass flow rate of 4.54 kg/s, and the maximum limit selection of 1.5% is due to the expected practical limitations as the injection velocities exceed the sonic values.

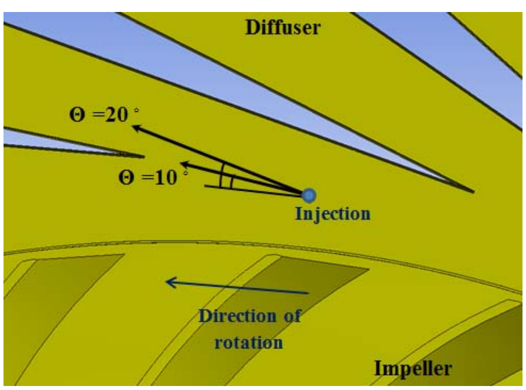

Figure 16. Description of the used air injection angles

Using different combinations of air injection parameters led to various results regarding modification of the stall cells. Table 1 shows the number of affected or disturbed diffuser passages for several cases of injection angles and injection mass flow rates. It may be noted from table 1 that the number of disturbed diffuser passages are decreasing by increasing the injection mass flow rate, and also by using of injection angle of 20° gives better results than the using of angle of 10°, and the best case among all the injection cases is the injection with angle of 20° at injection mass flow rate of 1.5%.

Table 1. Number of the affected diffuser passages for several cases of injection

		Injection angle	
		10°	20°
Injection mass flow rate (% of inlet design flow rate)	0.70%	5	4
	1%	4	3
	1.50%	4	1

The formation of localized high pressure regions during stall causes pressure fluctuation with time or in other words; impeller blades are exposed to force fluctuations with time. Figure 17 shows the force acting on impeller blades and its variation with time during stall in the axial flow direction for the case of no injection and for the injection cases of 10° and 20° at the maximum injection flow rate of 1.5%. The axial direction is the axis of rotation of the compressor at which the force component is large comparing with force components in the tangential and radial directions.

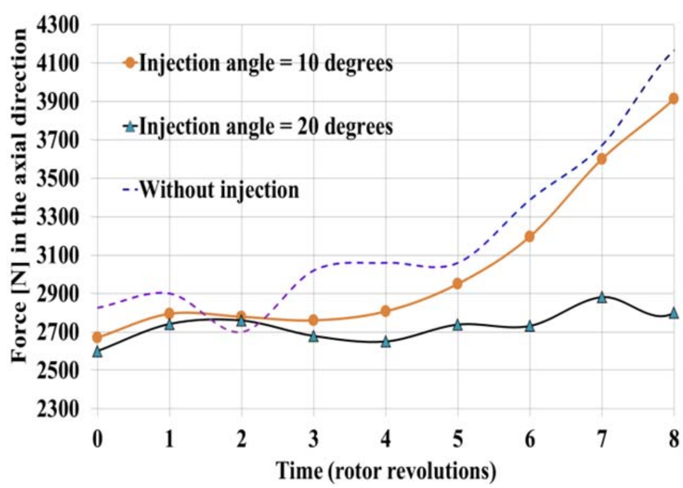

Figure 17. Force variation with time for various cases

Figure 17 shows that only the case of injection with angle of 20° has the force with small fluctuations with time and the force is not going to increase with time as for the cases of without injection and with using injection angle of 10°.

The role of air injection can be clarified by comparing flow behavior between the case of using injection and the case without using injection. Figures 18 and 20 show pressure distribution and velocity vectors respectively near the shroud surface during the stall development at a region affected by stall near the shroud surface for the case without using injection, while figures 19 and 21 show pressure distribution and velocity vectors respectively for the same region for the case of injection at angle of 20° and mass flow rate of 1.5%.

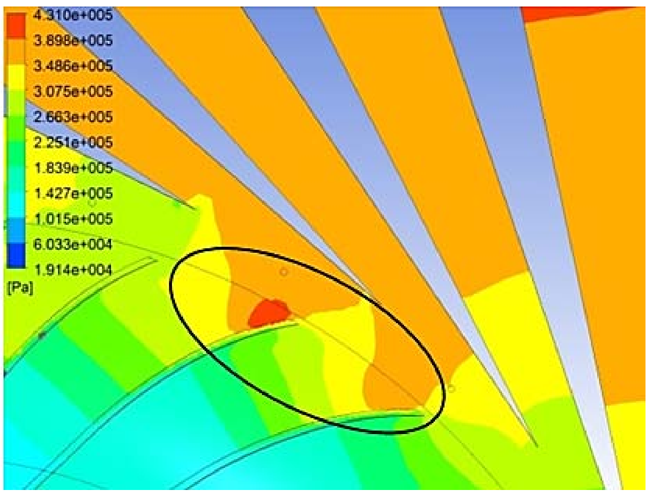

Figure 18. Pressure contours near shroud for the case of without injection

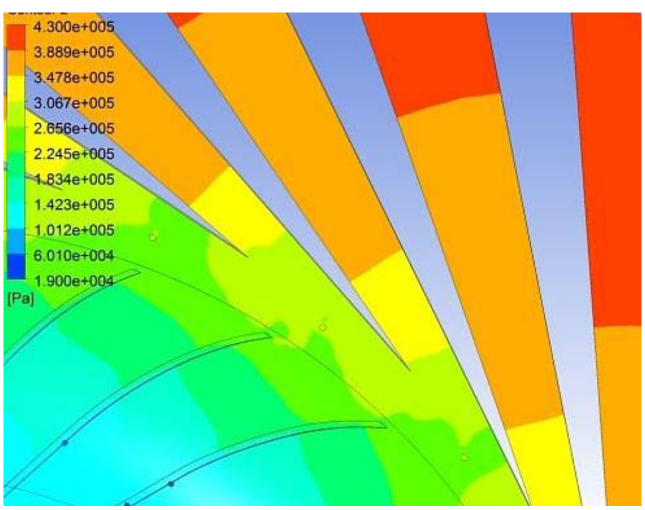

Figure 19. Pressure contours near shroud for the case of injection at angle of 20°

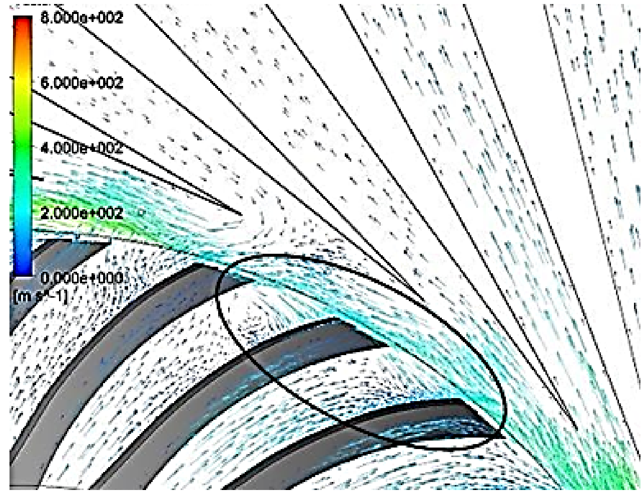

Figure 20. Velocity vectors near shroud for the case of without injection

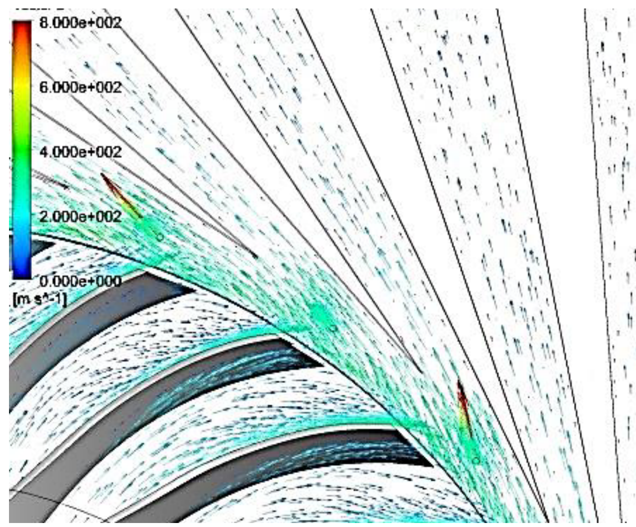

Figure 21. Velocity vectors near shroud for the case of injection at angle of 20°

Figure 18 shows that there is a high pressure region at the impeller exit (inside the ellipse shown on the figure), and the reason for this is the back flow coming from the diffuser and impacting the blade as can be seen from Fig.20. The effect of air injection is clear that the disturbed flow at the vaneless region is corrected as shown in Fig.21 that the velocity vectors direction is towards the diffuser passage, and this leads to the normal and identical pressure distribution in the diffuser passages (Fig.19).

6. CONCLUSIONS

(1) Flow separations at impeller blades cause the initiation of stall cells but the tip leakage flow is the main cause of stall development.
(2) During stall, the flow is weak at the vaneless region, and this results in failure of the fluid to enter some diffuser passages and leads to the initiation of back flow which moves to hit the impeller blades forming high pressure regions at the impact areas. These high pressure regions generate a force which pushes the fluid to move to the lower pressure areas at blades suction side through the tip clearance which is called the tip leakage flow. For the above reason, it can be concluded that controlling fluid at the vaneless region can prevent diffuser back flow and then prevent the tip leakage flow which causes stall development.
(3) Increasing the injection mass flow rate reduces the number of stall cells for the case of using injection angle of 20° but for the case of using injection angle of 10°, the number of stall cells is nearly constant. Accordingly, it may be concluded that increasing the injection mass flow rate is effective only for specified angles of injection; and this can be related to the degree of modification of velocity triangle at impeller exit due to the injected air.
(4) Using air injection at an angle of 20° and injection mass flow rate of 1.5% of the inlet design mass flow rate stabilized the compressor and prevented the stall development at mass flow rate of 3.8 kg/s (corresponding to a point inside the surge region) comparing with the case with injection angle of 10° and with the case of without injection.
(5) The injection mass flow rate is an important factor for the evaluation of the injection efficiency. In the current paper, three values for the injection mass flow rate of 0.7%, 1% and 1.5% of the design mass flow rate were discussed. It is recommended as a future work to study wide range of the injection mass flow rate values for each angle of injection in order to find the best effective value which can give the peak injection performance.

ACKNOWLEDGMENTS

This research was supported by a NPRP grant No. 4-651-2-242 from the Qatar National Research Fund (a member of Qatar Foundation), Doha, Qatar.

REFERENCES

[1] J. M. Haynes, G. J. Hendricks, and A. H. Epstein, "Active stabilization of rotating stall in a three-stage axial compressor," *ASME Transactions Journal of Turbomachinery,* vol. 116, pp. 226-239, 1994.
[2] N. M. McDougall, N. Cumpsty, and T. Hynes, "Stall inception in axial compressors," *Journal of Turbomachinery,* vol. 112, pp. 116-125, 1990.
[3] M. Tryfonidis, "A study of the rotating-stall inception in high-speed compressors," Massachusetts Institute of Technology, 1994.
[4] J. D. Paduano, E. Greitzer, and A. Epstein, "Compression system stability and active control," *Annual review of fluid mechanics,* vol. 33, pp. 491-517, 2001.
[5] I. Day, "Stall inception in axial flow compressors," *Journal of Turbomachinery,* vol. 115, pp. 1-9, 1993.
[6] Y. Ohta, Y. Fujita, and D. Morita, "Unsteady behavior of surge and rotating stall in an axial flow compressor," *Journal of Thermal Science,* vol. 21, pp. 302-310, 2012.
[7] M. P. Wernet, M. M. Bright, and G. J. Skoch, "An investigation of surge in a high-speed centrifugal compressor using digital PIV," *TRANSACTIONS-AMERICAN SOCIETY OF MECHANICAL ENGINEERS JOURNAL OF TURBOMACHINERY,* vol. 123, pp. 418-428, 2001.
[8] Y. Zhang, X. Lu, W. Chu, and J. Zhu, "Numerical investigation of the unsteady tip leakage flow and rotating stall inception in a transonic compressor," *Journal of Thermal Science,* vol. 19, pp. 310-317, 2010.
[9] C. Tan, I. Day, S. Morris, and A. Wadia, "Spike-type compressor stall inception, detection, and control," *Annual review of fluid mechanics,* vol. 42, pp. 275-300, 2010.
[10] H. D. Vo, C. S. Tan, and E. M. Greitzer, "Criteria for spike initiated rotating stall," *Journal of Turbomachinery,* vol. 130, 2008.
[11] S. Geng, F. Lin, J. Chen, and C. Nie, "Evolution of unsteady flow near rotor tip during stall inception," *Journal of Thermal Science,* vol. 20, pp. 294-303, 2011.
[12] M. Vagani, A. Engeda, and M. Cave, "Prediction of impeller rotating stall onset using numerical simulations of a centrifugal compressor. Part 1: Detection of rotating stall using fixed-flow transient simulations," *Proceedings of the Institution of Mechanical Engineers, Part A: Journal of Power and Energy,* 2013.
[13] B. Beheshti, B. Farhanieh, K. Ghorbanian, J. Teixeira, and P. Ivey, "Performance enhancement in transonic axial compressors using blade tip injection coupled with casing treatment," *Proceedings of the*

Institution of Mechanical Engineers, Part A: Journal of Power and Energy, vol. 219, pp. 321-331, 2005.
[14] H. Khaleghi, M. Boroomand, J. Teixeira, and A. Tousi, "A numerical study of the effects of injection velocity on stability improvement in high-speed compressors," *Proceedings of the Institution of Mechanical Engineers, Part A: Journal of Power and Energy,* vol. 222, pp. 189-198, 2008.
[15] I. Benhegouga and Y. Ce, "Steady Air Injection Flow Control Parameters in a Transonic Axial Compressor," *Research Journal of Applied Sciences,* vol. 5, 2013.
[16] J.-P. Chen, R. S. Webster, M. D. Hathaway, G. P. Herrick, and G. J. Skoch, "High performance computing of compressor rotating stall and stall control," *Integrated Computer-Aided Engineering,* vol. 16, pp. 75-89, 2009.
[17] G. Skoch, "Experimental Investigation of Diffuser Hub Injection to Improve Centrifugal Compressor Stability," *Journal of Turbomachinery,* pp. 107-117, 2005.
[18] G. J. SKOCH, "Experimental investigation of centrifugal compressor stabilization techniques," *Journal of Turbomachinery,* vol. 125, pp. 704-713, 2003.
[19] G. J. Skoch, P. Prahst, M. Wernet, J. Wood, and A. Strazisar, "Laser Anemometer Measurements of the Flow Field in a 4: 1 Pressure Ratio Centrifugal Impeller," DTIC Document1997.
[20] Z. Spakovszky, "Backward Traveling Rotating Stall Waves in Centrifugal Compressors (2002-GT-30379)," *Journal of Turbomachinery,* pp. 1-12, 2004.
[21] D. L. Tarr, "Scaling of impeller response to impeller-diffuser interactions in centrifugal compressors," Massachusetts Institute of Technology, 2008.
[22] T. F. McKain and G. J. Holbrook, *Coordinates for a high performance 4: 1 pressure ratio centrifugal compressor*: National Aeronautics and Space Administration, 1997.
[23] A. FLUENT, "13.0. ANSYS," *Inc., Canonsburg, PA, USA,* 2011.